Interactions Between Topological Defects and Nanoparticles

Syou-P'Heng Do, Amine Missaoui, Alessandro Coati, Andrea Resta, Nicolas Goubet, Sebastien Royer, Géraldine Guida, Emrick Briand, Emmanuel Lhuillier, Yves Garreau, et al.

frontiers in Physics

ORIGINAL RESEARCH
published: 06 February 2020
doi: 10.3389/fphy.2019.00234

Interactions Between Topological Defects and Nanoparticles

*Syou-P'heng Do[1], Amine Missaoui[1], Alessandro Coati[2], Andrea Resta[2], Nicolas Goubet[1], Sébastien Royer[1], Geraldine Guida[3], Emrick Briand[1], Emmanuel Lhuillier[1], Yves Garreau[2,4], David Babonneau[5], Michel Goldmann[1,2], Doru Constantin[6], Bernard Croset[1], Bruno Gallas[1] and Emmanuelle Lacaze[1]**

[1] Sorbonne Université, Faculté des Sciences, CNRS, Institut des Nano-Sciences de Paris (INSP), Paris, France, [2] Synchrotron Soleil, BP 48, L'Orme des Merisiers, Gif sur Yvette, France, [3] LEME, EA 4416, Universite Paris Nanterre, Nanterre, France, [4] Université de Paris, Laboratoire Matériaux et Phénomènes Quantiques, CNRS, Paris, France, [5] Institut Pprime, Département Physique et Mécanique des Matériaux, UPR 3346 CNRS, Université de Poitiers, Poitiers, France, [6] Laboratoire de Physique des Solides, Bat. 510, UMR-CNRS 8502, Université Paris-Sud, Université Paris-Saclay, Orsay, France

Liquid Crystal (LC) topological defects have been shown to trap nanoparticles (NPs) in the defect cores. The LC topological defects may thus be used as a matrix for new kinds of NP organizations templated by the defect geometry. We here study composites of LC smectic dislocations and gold NPs. Straight NP chains parallel to the dislocations are obtained leading to highly anisotropic optical absorption of the NPs controlled by light polarization. Combining Grazing Incidence Small Angle X-ray scattering (GISAXS), Rutherford Back Scattering (RBS), Spectrophotometry and the development of a model of interacting NPs, we explore the role of the Np size regarding the dislocation core size. We use NPs of diameter $D = 6$ nm embedded in an array of different kinds of dislocations. For dislocation core larger than the NP size, stable long chains are obtained but made of poorly interacting NPs. For dislocation core smaller than the NP size, the disorder is induced outside the dislocation cores and the NP chains are not equilibrium structures. However we show that at least half of these small dislocations can be filled, leading to chains with strongly enhanced electromagnetic coupling between the NPs. These chains are more probably stabilized by the elastic distortions around the defect cores, the distortion being enhanced by the presence of the grain boundary where the dislocations are embedded.

Keywords: liquid crystals, nanoparticles, topological defects, smectic dislocations, gold, LSP resonance

OPEN ACCESS

Edited by:
Uroš Tkalec,
University of Ljubljana, Slovenia

Reviewed by:
Ingo Dierking,
University of Manchester,
United Kingdom
Julio Cesar Armas-Perez,
University of Guanajuato, Mexico

***Correspondence:**
Emmanuelle Lacaze
emmanuelle.lacaze@insp.upmc.fr

Specialty section:
This article was submitted to Soft Matter Physics, a section of the journal Frontiers in Physics

Received: *19 September 2019*
Accepted: *16 December 2019*
Published: *06 February 2020*

Citation:
Do S-P, Missaoui A, Coati A, Resta A, Goubet N, Royer S, Guida G, Briand E, Lhuillier E, Garreau Y, Babonneau D, Goldmann M, Constantin D, Croset B, Gallas B and Lacaze E (2020) Interactions Between Topological Defects and Nanoparticles. Front. Phys. 7:234. doi: 10.3389/fphy.2019.00234

1. INTRODUCTION

Composites made of liquid crystals (LCs) and nanoparticles (NPs) are studied a lot nowadays [1–5]. One idea is to allow for controlled modification of the LC properties, which can be photonic properties but also elasticity, conductivity, magnetic properties or phase transition of LC [6–10]. The other idea is to take advantage of the anisotropy of the LC matrix or of its easy activation under external parameters (temperature, electric field) to build original anisotropic NP organizations [11, 12] or/and activable NP organizations [13]. Controlled NP organizations can allow for a control of plasmonic resonance when metallic NPs are concerned through the control of the nanorod orientation [14] or of the electromagnetic coupling between NPs for nanospheres and nanorods [11, 15]. In such a context LCs with topological defects have attracted attention because they might serve as templates for specific nanoparticle (NP) assemblies. Trapping of NPs within topological defect cores indeed allows for the release of the defect energy and the stabilization of the composite

systems [16–20]. As a result LC topological defects may be used for new kinds of NP organizations templated by the defect geometry [21–24]. In return the study of composites made of a LC matrix with topological defects and NPs can bring information on the topological defects themselves, in particular on the size, structure and energy of the defect core [3, 25], still mainly unknown [26].

In this article, we focus on smectic dislocations. Oriented arrays of smectic dislocations are formed in the so-called smectic oily streaks [27]. Composites made of smectic oily streaks and gold NPs have been shown to lead to the formation of NP chains, for gold nanospheres [11, 21] and end-to-end oriented gold nanorods [15], trapped in the linear and oriented dislocation cores. NP chains are interesting specific assemblies because of their anisotropy but are not easy to obtain since under Van der Waals interactions nanospheres form hexagonal networks, whereas nanorods form side by side assemblies. In the case of metallic NP chains, Localized Surface Plasmon (LSP) resonance becomes highly anisotropic and controlled by light polarization [11, 15, 21]. The trapping process by topological defect cores can be not only generalized to different NP shapes (from NP spheres to NP rods) but also to different NP natures. It has been shown that semiconducting nanorods also are oriented along a single direction in smectic oily streaks. The release of disorder core energy does not depend on the shape and on the NP nature. It thus allowed for the control of the polarization of semiconducting single-photon emitters [12]. We now explore the role of the NP size. The trapping efficiency by defect cores is expected to decrease when the NP size becomes larger than the defect core [28]. We study composites made of gold NPs of diameter $D =$ 6 nm in smectic oily streaks composed of an array of different kinds of dislocations in order to confront the respective roles of NP size and dislocation core size. Using combined Grazing Incidence Small Angle X-ray scattering (GISAXS), Rutherford Back Scattering (RBS), Spectrophotometry and the development of a model of interacting NPs, we compare the structure and stability of NP chains formed in dislocations of different core sizes. Different features are revealed depending on the respective sizes of NPs and dislocation cores. For large dislocations, larger than the NP size, long and stable NP chains are formed but with poorly interacting NPs. For small dislocations, a strong electromagnetic coupling between NPs occurs due to the disorder induced outside the dislocation core. However the NP chains maybe not an equilibrium state but instead a metastable state stabilized by the large elastic distortion around the dislocation core.

2. MATERIALS AND METHODS

2.1. NP Synthesis

1, 2, 3, 4-tetrahydronaphthalene (tetralin, 99% Aldrich), Chlorotriphenylphosphine Au (I) (98%) and tert-butylamine borane (97%) were obtained from STEM chemicals. Dodecanethiol (DDT), oleylamine, HAuCl4 (98%), hexane, were obtained from Sigma-Aldrich, Toluene (98%) from Riedel de Haen. Ethanol (99.85%), chloroform (99.2%) from VWR. All reagents were used as received without further purification. For the NPs of diameter $D = 6$ nm the synthesis is based on reference [29]. Fifty mg of HauCl4 are mixed in a three neck flask with 5 mL of oleyalmine and 5 mL of tetralin and degassed at room temperature. The flask is dipped in an ice bath. The temperature controller is put in the ice bath rather than in the three neck flask. Meanwhile, 22 mg of tertbutylborane is mixed with 0.5 mL of oleylamine and 0.5 mL of tetratlin. The mixture is sonicated until the full dissolution of the salt. The three neck flask is put under Ar. The borane solution is injected promptly. The solution changes color to brown and then to purple. Sonication is continued for 36 min. 0.5 mL of DDT is added to stop the reaction growth. The content of the flask is mixed with 5 mL of ethanol and then centrifuged. The formed pellet is redispersed in toluene. NPs of diameter $D = 6$ nm and polydispersity 9% were obtained as shown by SAXS measurements performed on synchrotron Soleil.

2.2. Composite Film Preparation

The samples were created by depositing a droplet of a mixture of 8CB (4-n-octyl-4′-cyanobiphenyl, smectic LC at room temperature, $c = 0.02$ M) and gold NPs in toluene (concentration varying from 5.5×10^{10} NPs μL^{-1} to 1.6×10^{11} NPs μL^{-1}) onto a polyvinyl alcohol (PVA) polymer film, initially spin-coated and rubbed on a glass substrate (1.8 cm^2).

2.3. Optical Microscopy and Micro-Spectroscopy Techniques

We measure the extinction properties of the samples using a Maya 2000 pro spectrometer coupled to an upright optical microscope (Leica DMRX) to probe 40×40 μm^2 areas. The signal was collected through an air objective ($\times 50$, NA $= 0.85$). The composite films were excited with linearly polarized light either along or perpendicular to the oily streaks. To extract the wavelength associated with the LSPR, the normalized spectra were fitted with a gaussian curve.

2.4. Dipole Coupling Model

The distance between the nanoparticles associated with a given LSP resonance wavelength, λ was calculated using a dipole coupling model in the quasistatic approximation (NPs diameter $D \ll \lambda$) [30]. In this approximation the multipolar interactions between the nanoparticles as well as the retardance effect are not considered, this latter assumption being obviously correct due to the small size of the NPs. In this case the resonance condition is characterized by [30]:

$$\epsilon = \epsilon_m \frac{\sum +8\left(\frac{S}{D}+1\right)^3}{\sum -4\left(\frac{S}{D}+1\right)^3} \quad (1)$$

with ϵ the Au NP dielectric function, ϵ_m the dielectric function of an homogeneous surrounding medium. S is the lattice sum of the NPs assembly, the NPs being associated with punctual dipoles. S depends on the geometry of the assembly and accounts for the electromagnetic coupling between the NPs [31]. For an infinite chain of NPs with a polarization parallel to the chains, the sum in equation (1) is $S \approx 4.8$. For monolayers associated with an infinite hexagonal network, the sum S is $S \approx 5.5$ [31, 32].

The Au NP dielectric function was recalculated based on Johnson and Christy data [33] to take into account the small size effect and the influence of the chemical interface, leading to broadening and blue-shifted LSPR of the isolated NPs in toluene (**Figure S1**) [21, 34].

2.5. Finite Element Calculations

For the calculations based on finite elements we have used the commercial software HFSS by ANSYS. Different chains of N nanoparticles with a diameter $D = 6$ nm and separated by a gap s were modeled. The number of particles was varied between 2 and 10 and the gap between 1 and 6 nm. The nanoparticles were modeled as spheres with the optical constants of gold and placed in the centre of a $400 \times 400 \times 400\,\text{nm}^3$ box filled with a medium with a constant refractive index of 1.51. Radiating boundaries were applied to the box and a plane wave polarized along the chain of nanoparticles was used as illumination. The optical response was calculated between 460 and 660 nm then the ohmic losses integrated over all the nanoparticles were computed to determine the position of the plasmon resonance.

2.6. X-Ray Diffraction

X-ray diffraction measurements were carried out at the SIXS beamline on the SOLEIL synchrotron facility. On SIXS beamline, the photon energy was fixed to 18 keV and the X-ray beam size to $300 \times 300\ \mu\text{m}^2$. The measurements were performed with the substrate almost parallel to the X-ray beam, in GISAXS (Grazing Incidence Small Angle X-ray Scattering) configuration [11].

2.7. Rutherford Backscattering Spectroscopy

The Rutherford Backscattering Spectrometry measurements were performed with the 2.2 MV Van de Graaff accelerator of the SAFIR platform of Sorbonne Université. RBS measurements were performed by positioning the samples perpendicularly to a beam of alpha particles with an energy of 1,800 keV, a diameter of 0.5 mm, a current of 40 nA and a charge of 4 μC. The measurements were performed with the ion beam incident normal to the sample surface and the backscattered ions were detected by a surface-barrier detector placed at a scattering angle of 165°. The energy calibration and solid angle of the detector are deduced from the measurement of a reference sample of 5.64×10^{15} bismuth atoms cm^{-2} implanted into silicon.

3. SMECTIC OILY STREAKS

We have used arrays of oriented defects of 8CB (4′-octyl-4-biphenylcarbonitrile) thin films deposited on rubbed poly(vinyl alcohol) (PVA) surfaces, the so-called smectic oily streaks. Due to hybrid anchoring at the two interfaces (air/8CB and 8CB/PVA, respectively), the smectic layers become curved in flattened hemicylinders perpendicular to the anchoring on the substrate, itself defined by the rubbing of the PVA substrate (**Figure 1**) [35–37]. These flattened hemicylinders, with a typical periodicity of several hundreds of nanometers, can be detected by polarized optical microscopy between crossed polarizers, leading to the observation of parallel stripes (**Figure 1A**). Their internal structure has been determined using combined X-ray diffraction and ellipsometry measurements [27]. It is characterized by the presence of two rotating grain boundaries per hemicylinder, buried within the smectic film, which profile has been precisely established by X-ray diffraction (in red in **Figure 1B**) [27]. Along each rotating grain boundary, three edge dislocations parallel to the hemicylinder axis (i.e., oriented along the Ox direction—**Figure 1B**) are expected (blue points in **Figure 1B**). This is due to a different number of rotating and flat smectic layers from each part of the grain boundary. They are of different Burgers vector depending on their localization along the rotating grain boundary. A first dislocation of Burgers vector, b with $b/d = 2$ (d is the intra-smectic layer spacing) is located in the first half of the rotating grain boundary, the nearest to the substrate. The two other dislocations lie close to the summit of the rotating grain boundary ($b/s \approx 6$). They are separated from each other by a distance of ∼50 nm and it has been shown that the rotating grain boundary profile does not depend on the thickness of the smectic film [27].

4. CHAIN FORMATION

Gold NPs of diameter $D = 6$ nm, covered by dodecanethiol ligands, have been first deposited on rubbed PVA. As shown by GISAXS measurements obtained on Soleil synchrotron facility (SIXS beamline - see the section Materials and Methods) and in agreement with electron microscopy measurements (**Figure 2**), the NPs form an hexagonal network on the substrate. Three pairs of rods are observed, (10), $(\bar{1}0)$, (11), $(\bar{1}\bar{1})$ and (20), $(\bar{2}0)$, being in the ratio 1, $\sqrt{3}$ and 2. They are the signature of the hexagonal network. The position of the (10) rod at 0.92 nm^{-1} leads to an inter-NP gap $s = 1.93 \pm 0.05$ nm, in perfect agreement with other measurements from the literature [38–40]. s is slightly larger than the length of the straight dodecanethiol, 1.8 nm, showing that within the NP network the ligands could be not too distorted but at least they are strongly interdigitated. The light extinction curve (**Figure 2B**) displays the LSP resonance of the NPs organized in an hexagonal network at $\lambda = 558$ nm. In comparison with the LSP resonance of gold NPs dispersed in toluene ($\lambda_o = 516$ nm, **Figure S1**), a red-shift is evidenced, in relation with the electromagnetic coupling between the NPs in the hexagonal network. It can be used to extract the inter-NP gap value in the dipolar approximation considering that the hexagonal networks are large enough to be considered as infinite for the LSP properties (see Materials and Methods) [41–43]. The 1.9 nm value consistent with X-ray results is recovered by using an optical index of $n = 1.51$ indeed close to the one of disordered dodecanethiol ($n = 1.46$). This is in agreement with an optical index dominated by the grafted dodecanethiol ligands around the NPs [11, 44].

In contrast with NPs deposited on rubbed PVA without LC, when NPs are inserted in 8CB smectic oily streaks (see section Materials and Methods), the light extinction becomes anisotropic. **Figure 3A** shows a typical extinction spectrum (probed area of $40 \times 40\,\mu\text{m}^2$). For a polarization of the incident light perpendicular to the oily streaks (black spectrum), the extinction maximum is slightly shifted to a lower wavelength compared to the one of NPs dispersed in toluene ($\lambda_o = 516$ nm, **Figure S1**), with LSP resonance at $\lambda_\perp \approx 500$ nm. In contrast,

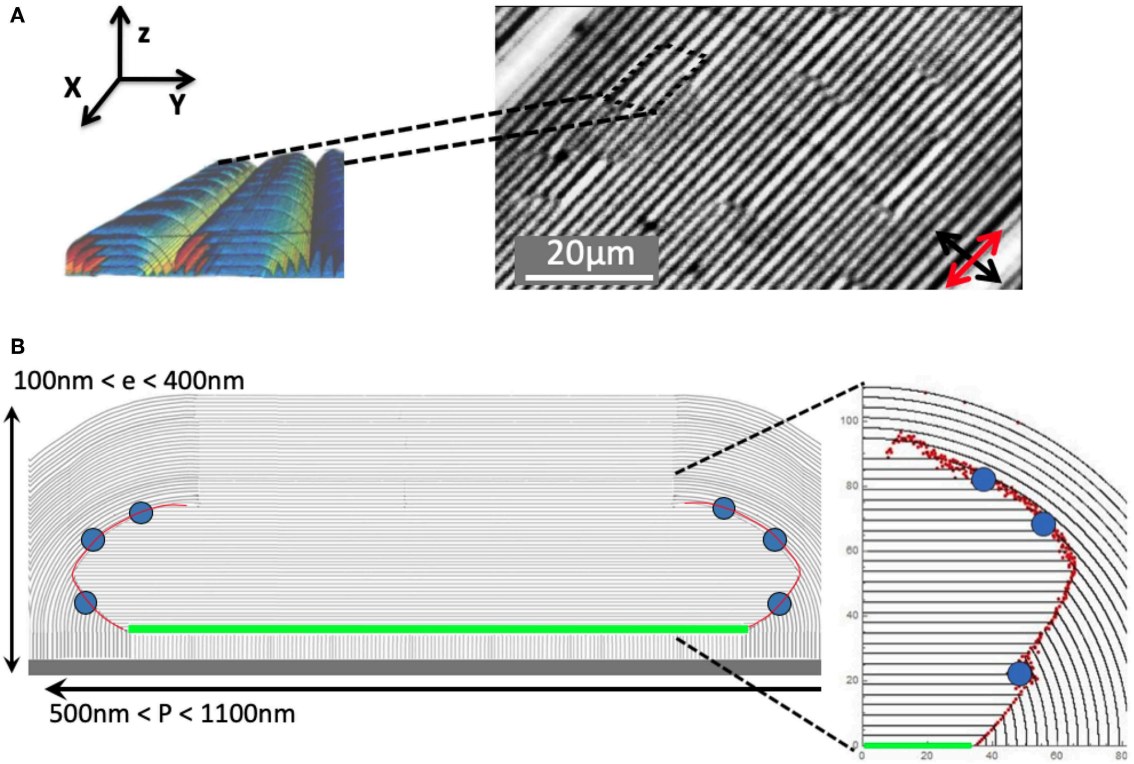

FIGURE 1 | (A) Polarized optical microscopy image of oily streaks observed from the top of a 150 nm-thick sample. Each stripe along OX corresponds to one hemicylinder and two hemicylinders in perspective are represented **(B)** Detail in side-view [in the (Y, Z) plane] of the smectic layers stacked in one given flattened hemicylinder for a typical thickness of 230 nm. Two rotating grain boundaries are shown in red, including dispersed edge dislocations (blue spots). A central grain boundary is underlined in green [27].

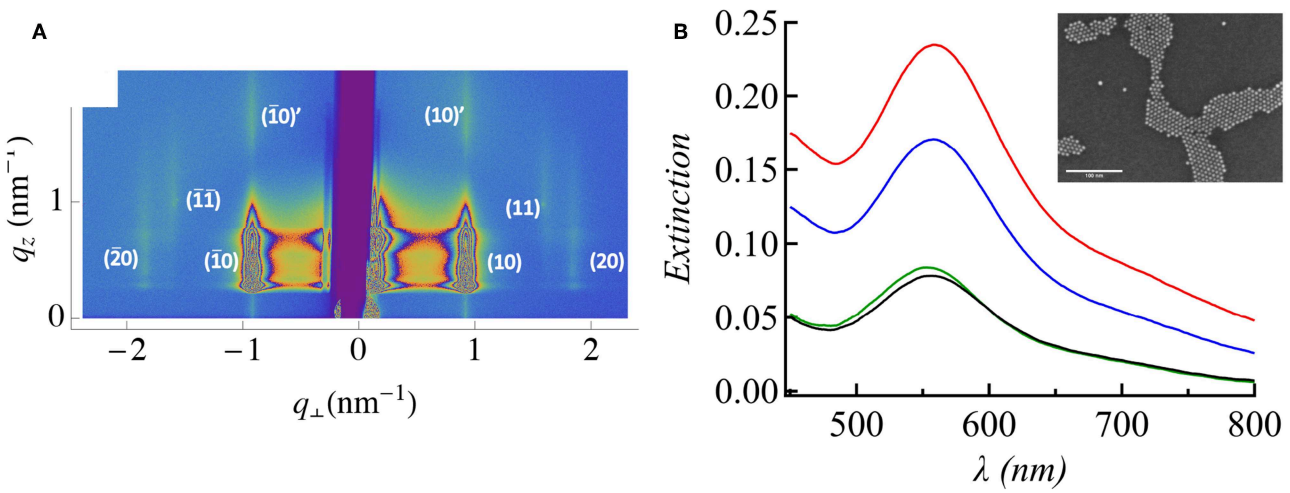

FIGURE 2 | (A) GISAXS signal of the NPs without LC, revealing the rods associated with the NP hexagonal network. **(B)** Light extinction of a network of NPs deposited on rubbed PVA substrate without LC. The LSP intensity varies depending on the measured area but not the wavelength resonance value ($\lambda = 558$ nm) except for the smallest intensity associated with the smallest NP domains. This demonstrates that, for $\lambda = 558$ nm, the hexagonal networks are large enough to be considered as infinite for the LSP properties. In inset is shown a Scanning Electron Microscopy (SEM) picture obtained with the same NPs when they were deposited on a Si substrate covered by rubbed PVA, also showing formation of an hexagonal network of NPs.

a clear red-shift of the LSP resonance is observed for a parallel polarization, with $\lambda_{\parallel} \approx 550$ nm. This indicates that a significant coupling between NPs occurs only in the direction parallel to the oily streaks, in relation with the formation of chains all parallel from each other and parallel to the dislocations [11, 21]. The spectral positions of extinction maxima taken from different zones of two samples are represented in red in the graph of $\lambda_{\parallel}$ as a function of $\lambda_{\perp}$ (**Figure 3B**). It appears that while $\lambda_{\perp}$ varies only little from one area to another, $\lambda_{\parallel}$ changes substantially, with a maximum for $\lambda_{\parallel}$ equal to 562 nm. This value for the chains is larger than the value obtained for the 2D monolayer without LC, $\lambda_{\parallel} = \lambda_{\perp} = 558$ nm. However for the same inter-NP gap and the same optical index, we would expect a higher LSP resonance wavelength for infinite NP hexagonal networks with respect to infinite NP chains. This latter wavelength is itself higher than for finite NP chains. The assumption of a same optical index in LC and without LC is very likely to be valid for two reasons: firstly it is known that the optical index is dominated by the grafted ligands with respect to the environment beyond the ligands [11, 44]. Secondly the optical index $n = 1.51$ should not be modified by the surrounding 8CB because the optical index expected in LC for a parallel polarization is close to the ordinary index of 8CB, $n_o = 1.52$, itself close to $n = 1.51$. The inter-NP gap in the NP chains formed in oily streaks is consequently in average smaller than without LC. There is a LC-induced shortening of the inter-NP gap in the NP chains. This result is in contrast with the same measurements made with smaller NPs of diameter $D = 4$ nm [11]. Either an equal or a larger inter-NP gap, depending on the preparation conditions, was obtained in the LC with respect to the network formed on rubbed PVA without LC [11].

5. CHAIN MODEL

In order to interpret these results, we consider that NP chain formation corresponds to a trapping of NPs in dislocations. The strength and efficiency of the linear trapping by dislocation cores has been previously highlighted by the fact that nanorods are aligned parallel to 8CB oily streaks. They are thus perpendicular to the nematic director but parallel to the defect cores, which is a strong indication of trapping by the linear defect cores [12, 15]. This is confirmed by the formation of NP chains, either made of nanorods [15] or of nanospheres of diameter $D = 4$ nm [11, 21]. We now observe the same phenomenon with larger NPs of diameter $D = 6$ nm but with a LC-induced shortening between NPs in contrast with NPs of diameter $D = 4$ nm. Trapping of NPs by dislocation cores may be kinetically favored by the known gradient of elastic distortion that attracts the NPs within the topological defect core [3, 19, 45]. However are the NP chains formed in the dislocation cores stable? In order to understand the structure and stability of NP chains, being trapped in dislocations, in particular the induced inter-NP gap that drives the electromagnetic coupling between the NPs, we have built a simple model that considers interacting NPs in LC. This model specifically takes into account the role of the LC in presence of topological defects. It is a model that has been built in order to understand the key parameters at the origin of the observed phenomena: NP chain formation and LC-induced shortening of the inter-NP gap. However since the interpretation of the details of the observed phenomena is not required, we have decided to only crudely consider the interaction of the NP chains with the surrounding LC, considering only two components: the favorable expulsion of disordered matter in the dislocation core; the unfavorable disorder induced by the NPs in LC if the NP size is larger than the dislocation core. We neglect in particular the details of the LC order variation and of the LC distortion around the defect core.

The energy of a NP chain made of N NPs separated by an inter-NP gap s, each NP being covered by a monolayer of ligands of length l (**Figure 4A**) can be estimated as follows: In a network of NPs, the equilibrium distance between the NPs is primarily controlled by the usual Van der Waals attraction between two NPs, balanced by the steric repulsion, both being mostly managed by the ligands around the NPs [46, 47]. We also have to take into account the mixing between the ligands leading to a model

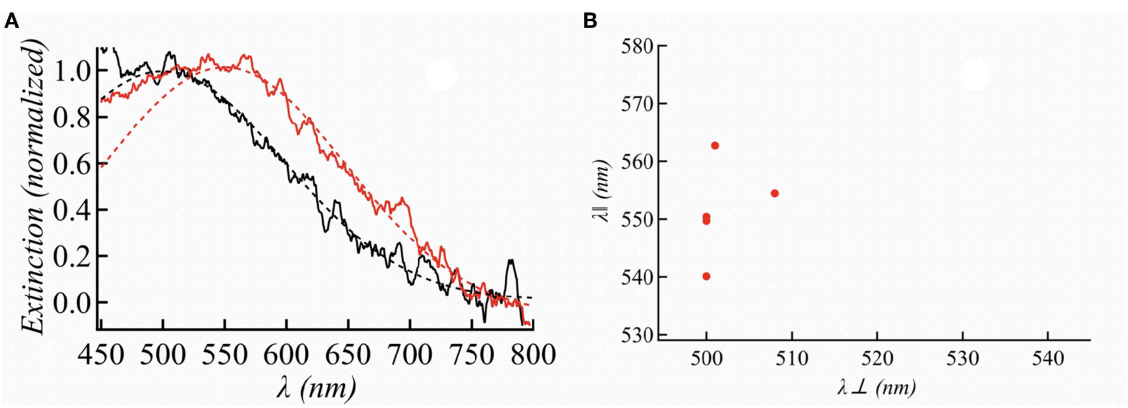

FIGURE 3 | (A) Normalized light extinction spectrum obtained in 8CB oily streaks containing gold NPs of diameter $D = 6$ nm. Superimposed gaussian fits are shown for the determination of the resonance wavelength. In black is the extinction for light polarization perpendicular to the 8CB oily streak stripes, in red for parallel polarization. **(B)** The different obtained extinction resonance measurements for NP chains represented by the $(\lambda_{\perp}, \lambda_{\parallel})$ values, obtained for NPs with diameter $D = 6$ nm embedded in 8CB oily streaks.

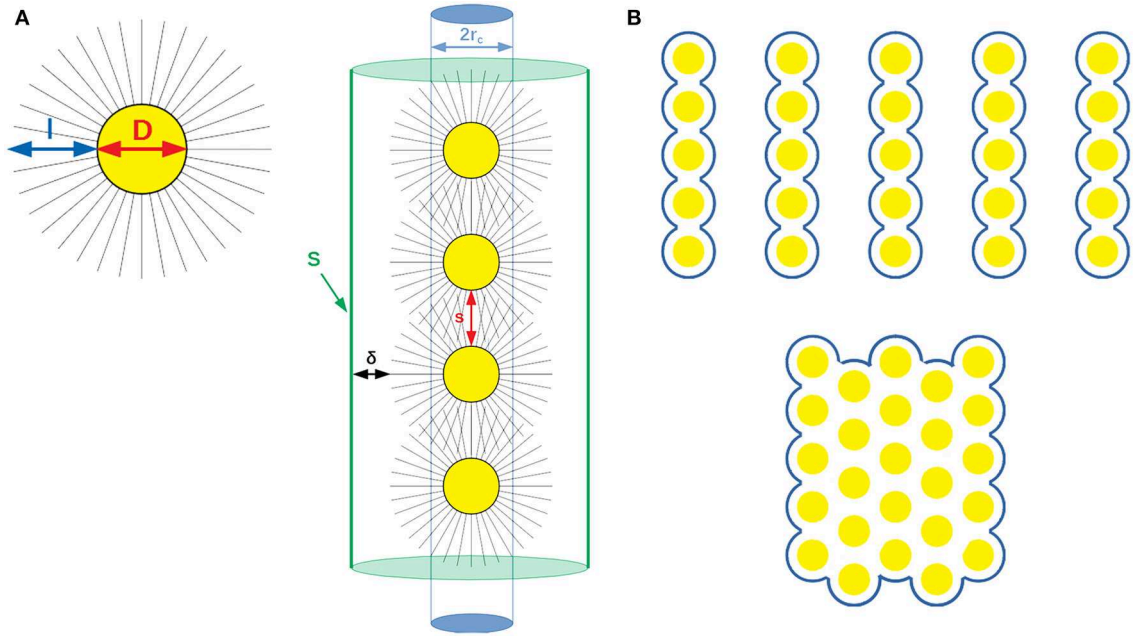

FIGURE 4 | (A) Model of the NPs with dodecanethiol ligands of length *l* and model of the NP chain with the disordered zone along the length δ shown beyond the ligands, of surface *S* shown in green. The dislocation core is schematically shown in blue. **(B)** Comparison of the surfaces of NP chains and NP FCC cube facets.

of interacting soft spheres [48]. In the case of ligands swollen by the solvent during the growth of the NP network, the usual parabolic curve of the energy of two interacting NPs is obtained as a function of *s*, the inter-NP gap [48]. If we consider toluene as solvent and gold NPs of diameter $D = 6$ nm covered by dodecanethiol, this leads to a well-marked equilibrium at $s = 1.9$ nm [38], in agreement with our combined X-ray and optical absorption measurements (**Figure 2**). In the presence of LC, two additional terms must be considered.

Firstly the energy related to the localization of the NP chain within the dislocation core, E_{Def}. This localization is favorable for the NPs since it allows the release of the disordered LC molecules of the core [16–18, 20]. As a result we expect the NPs to occupy the largest space as possible in the dislocation core to save the maximum of the dislocation core energy per unit of length, E_{DC} [11]. The length of the NP chain is $((N-1)(s+D)+D+2l)$ (**Figure 4A**). If the NP chain is embedded in the dislocation core of radius r_c, the volume of disordered matter, V_{DC} expelled by the presence of the NP chain is:

$$V_{DC} = \begin{cases} ((N-1)(s+D)+D+2l)\pi(D/2+l)^2, & if (D+2l) < 2r_c \\ ((N-1)(s+D)+D+2l)\pi r_c^2, & if (D+2l) > 2r_c \end{cases}$$

We can write:

$$E_{Def} = \begin{cases} -((N-1)(s+D)+D+2l)\frac{(D+2l)^2}{(2r_c)^2}E_{DC}, & if (D+2l) < 2r_c \\ -((N-1)(s+D)+D+2l)E_{DC}, & if (D+2l) > 2r_c \end{cases}$$

Secondly, the energy term related to the disorder induced by the NP within LC, E_{Dis}. It has already been shown that gold NPs of diameter $D = 4$ nm, covered by dodecanethiol ligands, may induce some disorder in a LC without topological defects. This disorder in return leads to a shortening of the inter-NP gap, in order to decrease in average the size of the LC disordered zone [49]. This disorder may be at the origin of the easy aggregation of NPs in LC, depending obviously on the nature of the ligands around the NPs [3, 50–52]. When the NP chains are embedded in the dislocation core, if the NP size $(D+2l)$ is strictly larger than the defect core diameter $2r_c$, we expect that some disorder may be created in the LC around the dislocation core. The volume of the disordered zone created in the LC, beyond the NP ligands is schematized on **Figure 4A**. The disorder may extend along a distance δ in the LC beyond the ligands. The disordered volume is thus equal to $\delta \times S_{chain}$, with S_{chain}, the surface of the disorder zone (see **Figure 4A**). If we neglect the surfaces at the extremities of the disordered cylinder since it may mainly correspond to the surface of the dislocation core, $S_{chain} = \pi(D+2l)(N-1)(D+s) + \pi(D+2l)^2$. There is an energy to pay for the creation of this disordered volume: $E_{dis} = \delta \times e_{dis} \times S_{chain}$, with e_{dis} the disorder energy per unit of volume. Consequently:

$$E_{dis} = \delta \times e_{dis} \times (\pi(D+2l)(N-1)(D+s) + \pi(D+2l)^2). \quad (2)$$

If $(D+2l) \leq 2r_c$, there is no disorder induced in LC in relation with NPs of size smaller or equal to the dislocation core, $E_{dis} = 0$. We only have to consider the overall energy $E(s) = (N-1)e(s) + E_{Def}$, with $e(s)$ the energy corresponding

to the soft sphere model for a given inter-NP gap, s [38, 48]. $dE/ds = 0$ and $dE_{Def}/ds = -(N-1)\frac{(D+2l)^2}{(2r_c)^2}E_{DC} < 0$ leading to a decrease of $de(s)/ds$ with respect to the equilibrium at $s = 1.9$ nm without LC. As a result, we expect an increase of s, the inter-NP gap, the NPs occupying the largest possible space within the dislocation core. This is the case of gold nanospheres covered by dodecanethiol of diameter $D = 4$ nm [11].

S_{FCC} being the surface of a FCC cube made of N^3 NPs. This suggests that:

$$N^2((n-1)(s+D)+D+2l)E_{DC} > (N^2(\pi(D+2l)(N-1)(D+s)+\pi(D+2l)^2) - S_{FCC})e_{dis}\delta \quad (5)$$

The calculation of the surface of a FCC cube thus leads to:

$$\pi(D+2l)\delta e_{dis} - E_{DC} < \delta e_{dis}\frac{N^2(D+s)^2(3/2+2\sqrt{3}) + N((\sqrt{3}+1)(s+D)\pi(D+2l) - 2(D+s)^2(3/2+2\sqrt{3}))}{N^3(s+D)+N^2(2l-s)+2(s+D)} + \delta e_{dis}\frac{(D+s)^2(3/2+2\sqrt{3}) - (\sqrt{3}+1)(s+D)\pi(D+2l) + 2\pi(D+2l)^2}{N^3(s+D)+N^2(2l-s)+2(s+D)} \quad (6)$$

If $(D+2l) > 2r_c$, the NP size is larger than the dislocation core size, disorder is induced outside the core. The equilibrium established without NPs becomes differently modified in LC. If $d/ds(E_{Def}+E_{dis}) = (N-1)(\pi(D+2l)\delta e_{dis} - E_{DC}) < 0$, s is increased; if $\pi(D+2l)\delta e_{dis} - E_{DC} > 0$, s is decreased. With NPs of diameter $D = 6$ nm, we find a decrease of s with respect to NP networks formed without LC in contrast with NPs pf diameter $D = 4$ nm. This brings two conclusions:

- In smectic oily streaks there are dislocations of core size intermediate between the NP sizes associated with gold diameters $D = 4$ nm and $D = 6$ nm.
- The corresponding dislocation core energy per unit of length, $E_{DC} < \pi(D+2l)\delta e_{dis}$, with $D = 6$ nm and l the length of the dodecanethiol in LC.

A second issue is: Are the NP chains equilibrium structures?

If $(D+2l) \leq 2r_c$, they are obviously equilibrium structures. The energy of N NPs potentially inducing disorder in LC is reduced when they are embedded in the dislocation core.

If $(D+2l) > 2r_c$, this is not obvious. As shown by **Figure 4B**, the surface of the disordered zone induced by a FCC cube of edge made of N NPs is clearly smaller than the one of N^2 chains made of N NPs. This should favor aggregation of NPs instead of formation of NP chains trapped in dislocation cores, except if the dislocation core energy per unit of length, E_{DC} is large enough to compensate the disorder induced by a chain outside the defect core. To obtain formation of stable chains, we expect for N^2 chains made of N NPs, neglecting the variation of entropy between N^2 chains and a single FCC cube:

$$N^2(S_{chain}\times e_{dis}\times\delta - ((N-1)(s+D)+D+2l)\times E_{DC}) < S_{FCC}\times e_{dis}\times\delta. \quad (3)$$

In other words:

$$N^2((\pi(D+2l)(N-1)(D+s)+\pi(D+2l)^2)e_{dis}\delta - ((N-1)(s+D)+D+2l)E_{DC}) < S_{FCC}\times e_{dis}\times\delta \quad (4)$$

If N is large enough this transforms into:

$$\pi(D+2l)\delta e_{dis} - E_{DC} < \delta e_{dis}\left(\frac{(D+s)(3/2+2\sqrt{3})}{N} + \frac{(\sqrt{3}+1)\pi(D+2l) - 3(D+s)(3/2+2\sqrt{3})}{N^2}\right) \quad (7)$$

With the other inequality obtained above, we finally have:

$$0 < \pi(D+2l)\delta e_{dis} - E_{DC} < \delta e_{dis}\left(\frac{(D+s)(3/2+2\sqrt{3})}{N} + \frac{(\sqrt{3}+1)\pi(D+2l) - 3(D+s)(3/2+2\sqrt{3})}{N^2}\right) \quad (8)$$

This result shows that it is not possible to create very long chains (N close to infinity) being equilibrium structures. The decreasing of the inter-NP gap in the NP chains observed in the smectic oily streaks is indeed driven by the value of $\pi(D+2l)\delta e_{dis} - E_{DC}$ that can not be strictly zero. To create equilibrium long chains (N large), the dislocation core energy per unit of length, E_{DC} must be close to $e_{dis}\delta\pi(D+2l)$. In order to satisfy both inequalities e_{dis} and E_{DC} must be large enough.

6. DISCUSSION

Smectic oily streaks are composed of 2 similar dislocations at the summit of the rotating grain boundary (Burgers vector b, $b/d \approx 6$, with d the inter-smectic layer spacing, $d = 3.16$ nm in 8CB), coexisting with another dislocation, of smaller Burgers vector (Burgers vector b, $b/d \approx 2$) nearer to the substrate (**Figure 1B**). The diameter of the dislocation cores, $2r_c$ is generally expected to be close to the dislocation Burgers vector [53, 54]. With a Burgers vector $b/d = 1$, $2r_c$ has indeed been shown to be very close to d for smectic C edge dislocations [55] and for smectic A screw dislocations [56]. If the NPs would induce disorder outside the defect core for the three dislocations of the oily streaks, this would imply that all the dislocation core radii would be smaller than the half of the NP size $D+2l$ with l the dodecanethiol length in 8CB. The dodecanethiol length in 8CB is not known but can be considered as ranging between 1 nm, its highly stretched value [46] and 1.8 nm its extended value. $(D+2l) \approx$ 8–10 nm

is not more than 3 times d, the 8CB inter-smectic layer spacing. This is largely too small to account for two times the core radius of a dislocation of Burgers vector b such that $b/d \approx 6$. This demonstrates that the hypothesis of only one kind of dislocation inducing disorder outside the core is highly more probable. It must be the smallest one, the dislocation of Burgers vector b, with $b/d \approx 2$ and we finally obtain an estimation of the corresponding dislocation core radius, r_c. $2r_c$ may range between the NP size associated with the gold diameter $D = 4$ nm and the NP size with the diameter $D = 6$ nm. Considering the dodecanethiol length as ranging between 1 and 1.8 nm, this leads to 6 nm $< 2r_c <$ 9.6 nm. The fact that similar LC-induced decrease in the inter-NP gap has been observed for NP diameters $D = 5$ nm (see **Figure S2**) even allows to decrease the inequality to 6 nm $< 2r_c <$ 8.6 nm. This is in very good agreement with the presence of dislocations of core radius, r_c such that $2r_c \approx 2d = 6.3$ nm, in smectic oily streaks, associated with a Burgers vector b, with $b/d = 2$.

As a result, the preferred dislocations for NP trapping are the largest dislocations where the largest amount of disorder energy is saved in the presence of NPs and no disorder is induced outside the defect core. They are equilibrium structures for NPs of diameter $D = 6$ nm. The smallest dislocations may be filled by NPs at high NP concentration only when the largest dislocations may be already significantly filled. A large number of NPs is thus required to explain the observed decrease of inter-NP gap revealed by the $\lambda_{\parallel}$ measurements of the NP chains shown in **Figure 3B**. We have used Rutherford Backscattering Spectroscopy (RBS) experiments (see Materials and Methods) to obtain the average number of gold atoms in the smectic oily streaks. We have found in average 1300 NPs μm^{-2} for one of the two samples presented in **Figure 3B**. Assuming an inter-NP distance of $D + 1.4 = 7.4$ nm, 1.4 nm being the average inter-NP gap in the chains (see below), it can be calculated that a linear defect of length 1 μm contains up to approximately 140 NPs. As a result, for the LC thickness of 170 nm found for the corresponding composite oily streak sample, the period of oily streaks being of the order of 550 nm [27], the critical concentration necessary to entirely fill the 6 dislocations of one hemicylinder (**Figure 1B**) is 1530 NPs μm^{-2}. 1300 NPs μm^{-2} corresponds to 85% of the 6 linear dislocations shown in **Figure 1B** being fully filled by NPs confirming a significant filling of the small dislocations in addition to the large ones. If we consider the large dislocations as being almost fully filled by NPs, this leads to a half filling on average for the small dislocations.

Despite the larger NP filling in large dislocations, the average LSP measurements of highest $\lambda_{\parallel}$ presented in **Figure 3** are expected to be dominated by the NP chains in the small dislocations. These latter chains are the only ones subjected to strong electromagnetic coupling between NPs. $\lambda_{\parallel} = 550$ nm is the LSP resonance value calculated in the dipolar approximation with infinite chains of inter-NP gap $s = 1.9$ nm and with a dipolar index $n = 1.51$, 1.9 nm corresponding to the equilibrium inter-NP gap without LC. The expected increase of the inter-NP gap in the large dislocations without induced disorder outside the defect core should lead to $\lambda_{\parallel}$ significantly smaller than $\lambda_{\parallel} = 550$ nm. In agreement with coexisting NP chains of large inter-NP gaps in large dislocations together with NP chains of small inter-NP gaps in small dislocations, all extinction data are enlarged toward the low wavelength values (**Figure 3A**), the low wavelength values being associated with the NP chains in the large dislocations. In contrast the maximum $\lambda_{\parallel}$ shown in **Figure 3B**, $\lambda_{\parallel} = 562$ nm may be dominated by the NP chains trapped in the small dislocations. $\lambda_{\parallel}$ ranging between 540 and 562 nm as shown on **Figure 3B** may be associated with different local concentrations of NPs in the small dislocations. This may be associated with different lengths of NP chains in the small dislocations for a same sample of average filling of the dislocations of 85%.

The average length of the NP chains in the small dislocations is not known. In order to use the maximum $\lambda_{\parallel}$ of 562 nm to extract an inter-NP gap value and use it for an estimation of the energy per unit of length of the small dislocations, E_{DC}, with the assumption that they form equilibrium structures, we have considered different possible average lengths for the NP chains. If the chains are long enough to be considered as infinite for LSP properties [41–43], the dipolar approximation with a dipolar index $n = 1.51$ leads to $s = 1.4$ nm. For numbers of NPs in the chains, N, which can not be considered as infinite, the wavelengths of the LSP resonances of chains of gold NPs were calculated with finite element methods (see Materials and Methods). The variations $\Delta\lambda$ of the position of the LSP resonance of the NP chains with respect to the position for isolated NPs λ_o were then fitted to a plasmon ruler [57]:

$$\Delta\lambda = \lambda_o \beta e^{-\frac{\left(\frac{2s}{D(n-1)}\right)^{\nu}}{\tau}} \tag{9}$$

where the decay rate $\tau = 0.324$ the exponent $\nu = 0.55$ and the scaling parameter $\beta = 0.16$ were adjustable parameters. **Figure S3** gives the variations of the calculated $\Delta\lambda$ in nm as a function of $\frac{2s}{D(n-1)}$ together with the plasmon ruler.

We obtain $s = 1.3$ nm for $N = 10$. It is hard to account for an inter-NP gap smaller than $s = 0.6$ nm, the value that has been found without topological defects in cholesteric films with NPs of diameter $D = 4$ nm. This latter case, $s = 0.6$ nm, corresponds to $N = 5$. We can then use the previously calculated energy curve of interacting NPs without LC, $e(s)$, as a function of the inter-NP gap, s, for gold NPs of diameter $D = 6$ nm with grafted dodecanethiol in toluene [38]. It leads to the observed equilibrium inter-NP gap of $s = 1.9$ nm without LC but also gives the evolution of $e(s)$ in case of departure of s with respect to $s = 1.9$ nm. Using in LC the fact that:

$$\frac{d(e(s))}{ds} = -(\pi(D + 2l)\delta e_{dis} - E_{DC}) \tag{10}$$

allows to obtain:

If N = 10 and s = 1.3 nm [38], $\pi(D + 2l)\delta e_{dis} - E_{DC} = 16kTnm^{-1}$

If N = 5 and s = 0.6 nm [38], $\pi(D+2l)\delta e_{dis} - E_{DC} = 42kTnm^{-1}$

If the NP chains in the small dislocations are equilibrium structures they must also respect inequality (8), leading (with $l = 1.8$ nm) to:

$$\begin{cases} \pi(D + 2l)\delta e_{dis} > 145kTnm^{-1}, E_{DC} > 129kTnm^{-1}, \text{ if } N = 10 \\ \pi(D + 2l)\delta e_{dis} > 160kTnm^{-1}, E_{DC} > 118kTnm^{-1}, \text{ if } N = 5. \end{cases}$$

e_{dis} and E_{DC} necessary to obtain equilibrium NP chains consistent with the measured optical absorption in the composites oily streaks/gold NPs, $\lambda_{\parallel} = 562$ nm, finally only poorly depend on the NP chain length. They appear very large. With the rough assumption that the zone around the dislocation core is transformed into a nematic zone, in agreement with recent results obtained with a screw dislocation [56] and neglecting the elastic nematic distortion within this zone, e_{dis} is the Landau-de Gennes penalty: $e_{dis} = 0.73$ kT nm^{-3}, for 8CB at 25°C [58]. Taking l as 1.8 nm, we need $\delta \approx 6nm$ to reach $\pi(D + 2l)\delta e_{dis} > 145$kT nm^{-1} which is two times the intra-layer spacing. Measurements of the core energy of dislocations are still scarce. The total energy of dislocations, including the core energy, has been measured as a function of the Burgers vector in 8CB free standing films. It confirmed that it is proportional to the Burgers vector [59]. For a Burgers vector $b/d = 1$ the energy per unit of length is 5 kT nm^{-1} [59]. Here we find E_{DC} at least 16 times larger for a Burgers vector only two times larger. Such a large value may be due to the complex structure of oily streak dislocations associated with a large disorientation of the smectic layers from each part of the dislocation (**Figure 1**). Another assumption is that the NP chains in the small dislocations are not an equilibrium structure in relation with the induced disorder outside the core. They could be only kinetically favored by the attraction toward the defect core occurring due to the elastic distortion around the dislocations [3, 19, 45]. The fact that the dislocations are embedded in rotating grain boundaries may strongly enhance this phenomenon, through the presence of additional elastic distortion.

7. CONCLUSION

Combining GISAXS, spectrophotometry, RBS measurements and the development of a model of interacting NPs, we present a comprehensive description of composites made of gold NPs with a given diameter $D = 6$ nm in an array of different kinds of smectic dislocations (with different Burgers vectors). If the NP concentration is small, only the large dislocations are filled and long chains may be formed. They are favorable equilibrium structures because no disorder is induced outside the defect core but they consist of only poorly interacting NPs. If the NP concentration is large enough, the small dislocations can also be filled and we demonstrate up to 85 % of the dislocations being filled without any aggregation outside the core. We demonstrate that such high filling of the dislocations by the NPs leads to the coexistence of different NP chains in the smectic film, long NP chains with large inter-NP gap coexisting with smaller chains with a shortened inter-NP gap that can become as small as 1.4 nm. As a result the plasmonic properties of the composite are dominated by the small chains due to the LC-induced enhanced electromagnetic coupling between the NPs in the small dislocations. Using a model that takes into account the modifications of the interactions between NPs associated with their localization in the smectic dislocations, we confirm the presence of dislocations of Burgers vector b, $b/d = 2$, the "small" dislocations. We also demonstrate that the NP chains formed in the "small" dislocations are most probably not equilibrium structures. This is due to the disorder outside the defect core which is responsible for the observed LC-induced shortening inter-NP gap. However these NP chains might remain stable over time due to the elastic distortion around the rotating grain boundary that might play the role of the energy barrier for the trapped NPs.

DATA AVAILABILITY STATEMENT

The datasets generated for this study are available on request to the corresponding author.

AUTHOR CONTRIBUTIONS

All authors listed have made a substantial, direct and intellectual contribution to the work, and approved it for publication.

ACKNOWLEDGMENTS

We thank D. Limagne, C. Rafaillac, and B. Voisin for technical support. D. Demaille and L. Becerra for the electronic Microscopy; Y. Vickridge for the analysis of the RBS data. We thank CNES (Centre National d'Etudes Spatiales) for supporting this project. Concerning the financial funding, SD, AM, and EL thank the French state funds managed by the ANR within the Investissements d'Avenir programme under reference ANR-11-IDEX-0004-02, and more specifically within the framework of the Cluster of Excellence MATISSE. We also thank Synchrotron SOLEIL for providing the beam on SixS beamline.

SUPPLEMENTARY MATERIAL

The Supplementary Material for this article can be found online at: https://www.frontiersin.org/articles/10.3389/fphy.2019.00234/full#supplementary-material

Figure S1 | Extinction in toluene of the NPs of diameter 6 nm.

Figure S2 | The different obtained extinction measurements for NP chains represented by the ($\lambda_{\perp}$; $\lambda_{\parallel}$) values, obtained for NPs with diameter $D = 5$ nm, for which the extinction of hexagonal networks without LC is at $\lambda_{\perp} = \lambda_{\parallel} = 558$ nm.

Figure S3 | $2s/(N-1)D$ as a function of Delta lambda, calculated (in blue) with finite element method compared with the plasmon ruler (in red).

REFERENCES

1. Bisoyi HK, Kumar S. Liquid-crystal nanoscience: an emerging avenue of soft self-assembly. *Chem Soc Rev*. (2011) **40**:306–19. doi: 10.1039/B901793N
2. Lagerwall JPF, Scalia G. A new era for liquid crystal research: applications of liquid crystals in soft matter nano-, bio- and microtechnology. *Curr Appl Phys*. (2012) **12**:1387–412. doi: 10.1016/j.cap.2012.03.019
3. Blanc C, Coursault D, Lacaze E. Ordering nano-and microparticles assemblies with liquid crystals. *Liquid Cryst Rev*. (2013) **1:**83–109. doi: 10.1080/21680396.2013.818515
4. Lewandowski W, Wojcik M, Górecka E. Metal nanoparticles with liquid-crystalline ligands: controlling nanoparticle superlattice structure and properties. *ChemPhysChem*. (2014) **15**:1283–95. doi: 10.1002/cphc.201301194

5. Choudhary A, Singh G, Biradar AM. Advances in gold nanoparticle–liquid crystal composites. *Nanoscale*. (2014) **6**:7743–56. doi: 10.1039/C4NR01325E
6. Sridevi S, Prasad SK, Nair GG, D'Britto V, Prasad BLV. Enhancement of anisotropic conductivity, elastic, and dielectric constants in a liquid crystal-gold nanorod system. *Appl Phys Lett*. (2010) **97**:151913. doi: 10.1063/1.3499744
7. Mishra M, Kumar S, Dhar R. Effect of dispersed colloidal gold nanoparticles on the electrical properties of a columnar discotic liquid crystal. *RSC Adv*. (2014) **4**:62404–12. doi: 10.1039/C4RA11541D
8. Tomašovičová N, Timko M, Mitróová Z, Koneracká M, Rajňak M, Éber N, et al. Capacitance changes in ferronematic liquid crystals induced by low magnetic fields. *Phys Rev E*. (2013) **87**:014501. doi: 10.1103/PhysRevE.87.014501
9. Mouhli A, Ayeb H, Othman T, Fresnais J, Dupuis V, Nemitz IR, et al. Influence of a dispersion of magnetic and nonmagnetic nanoparticles on the magnetic Fredericksz transition of the liquid crystal 5CB. *Phys Rev E*. (2017) **96**:012706. doi: 10.1103/PhysRevE.96.012706
10. Ramanuj M, Jayanta H, Anil H, Binod G, Ragini D, Debanjan B, et al. Dielectric properties of a strongly polar nematic liquid crystal compound doped with gold nanoparticles. *Liquid Cryst*. (2018) **45**:1661–71. doi: 10.1080/02678292.2018.1478995
11. Coursault D, Blach JF, Grand J, Coati A, Vlad A, Zappone B, et al. Towards a control of anisotropic interactions between soft nanospheres using dense arrays of smectic liquid crystal edge dislocations. *ACS Nano*. (2015) **9**:11678–89. doi: 10.1021/acsnano.5b02538
12. Pelliser L, Manceau M, Lethiec C, Coursault D, Vezzoli S, Lemenager G, et al. Alignment of rod-shaped single photon emitters driven by line defects in liquid crystals. *Adv Funct Mater*. (2015) **25**:1719–26. doi: 10.1002/adfm.201403331
13. Lee E, Xia Y, Ferrier RC Jr, Kim HN, Gharbi MA, Stebe KJ, et al. Fine golden rings: tunable surface plasmon resonance from assembled nanorods in topological defects of liquid crystals. *Adv Mater*. (2016) **28**:2731–6. doi: 10.1002/adma.201506084
14. Liu Q, Yuan Y, Smalyukh II. Electrically and optically tunable plasmonic guest Host liquid crystals with long-range ordered nanoparticles. *Nanoletters*. (2014) **14**:4071. doi: 10.1021/nl501581y
15. Rozic B, Fresnais J, Molinaro C, Calixte J, Umadevi S, Lau-Truong S, et al. Oriented gold nanorods and gold nanorod chains within smectic liquid crystal topological defects. *ACSNano*. (2017) 11:6728–38. doi: 10.1021/acsnano.7b01132
16. Yoshida H, Tanaka Y, Kawamoto K, Kubo H, Tsuda, Fujii A, et al. Nanoparticle-stabilized cholesteric blue phases [Article]. *Appl Phys Express*. (2009) **2**:121501. doi: 10.1143/APEX.2.121501
17. Karatairi E, Rozic B, Kutnjak Z, Tzitzios V, Nounesis G, Cordoyiannis G, et al. Nanoparticle-induced widening of the temperature range of liquid-crystalline blue phases. *Phys Rev E*. (2010) **81**:041703. doi: 10.1103/PhysRevE.81.041703
18. Rozic B, Tzitzios V, Karatairi E, Tkalec U, Nounesis G, Kutnjak Z, et al. Theoretical and experimental study of the nanoparticle-driven blue phase stabilisation. *Eur Phys J E*. (2011) **34**:1–11. doi: 10.1140/epje/i2011-11017-8
19. Senyuk B, Evans JS, Ackerman PJ, Lee T, Manna P, Vigderman L, et al. Shape-dependent oriented trapping and scaffolding of plasmonic nanoparticles by topological defects for self-assembly of colloidal dimers in liquid crystals. *Nano Lett*. (2012) **12**:955–63. doi: 10.1021/nl204030t
20. Cordoyiannis G, Rao J i VS, Kralj S, Dhara S, Tzitzios V, Basina G, et al. Different modulated structures of topological defects stabilized by adaptive targeting nanoparticles. *Soft Matt*. (2013) **9**:3956–64. doi: 10.1039/c3sm27644a
21. Coursault D, Grand J, Zappone B, Ayeb Hand L'evi G, F'elidj N, Lacaze E. Linear self-assembly of nanoparticles within liquid crystal defect arrays. *Adv Matt*. (2012) 24:1461–5. doi: 10.1002/adma.201103791
22. Evans JS, Ackerman PJ, Broer DJ, van de Lagemaat J, Smalyukh II. Optical generation, templating, and polymerization of three-dimensional arrays of liquid-crystal defects decorated by plasmonic nanoparticles. *Phys Rev E*. (2013) **87**:032503. doi: 10.1103/PhysRevE.87.032503
23. Gharbi MA, Manet S, Lhermitte J, Brown S, Milette J, Toader V, et al. Reversible nanoparticle cubic lattices in blue phase liquid crystals. *ACS Nano*. (2016) **10**:3410–15. doi: 10.1021/acsnano.5b07379
24. Mundoor H, Sheetah GH, Park S, Ackerman PJ, Smalyukh II, van de Lagemaat J. Tuning and switching a plasmonic quantum dot sandwiched in a nematic line defect. *ACS Nano*. (2018) **12**:2580–90. doi: 10.1021/acsnano.7b08462
25. Lacaze E, Coursault D. Control of nanoparticle self-assemblies using distorted liquid crystals. In: Lagerwall JPF, Scalia G, editors. *Liquid Crystals with Nano and Microparticles. Series in Soft Condensed Matter*. Singapore: World Scientific (2016). p. 186–222.
26. Rahimi M, Ramezani-Dakhel H, Zhang R, Ramirez-Hernandez A, Abbott NL, de Pablo JJ. Segregation of liquid crystal mixtures in topological defects. *Nat Commun*. (2017) **8**:15064. doi: 10.1038/ncomms15064
27. Coursault D, Zappone B, Coati A, Boulaoued A, Pelliser L, Limagne D, et al. Self-organized arrays of dislocations in thin smectic liquid crystal films. *Soft Matter*. (2016) **12**:678–88. doi: 10.1039/C5SM02241J
28. Ravnik M, Alexander G, Yeomans J, Zumer S. Three-dimensional colloidal crystals in liquid crystalline blue phases. *Proc Natl Acad Sci USA*. (2011) **108**:5188–92. doi: 10.1073/pnas.1015831108
29. Peng S, Lee Y, Wang C, Yin H, Dai S, Sun S. A facile synthesis of monodisperse Au nanoparticles and their catalysis of CO oxidation. *Nano Res*. (2008) **1**:229–34. doi: 10.1007/s12274-008-8026-3
30. Kreibig U, Vollmer M. *Optical Properties of Metal Clusters*. Vol. 25. Springer Series in Materials Science. Springer (1995).
31. Topping J. On the mutual potential energy of a plane network of doublets. *Proc R Soc London A*. (1927) **114**:67–72. doi: 10.1098/rspa.1927.0025
32. Van der Hoff BME, Benson GC. A method for the evaluation of some lattice sums oocurring in calculations of physical properties of crystals. *Can J Phys*. (1953) 31:1087–04. doi: 10.1139/p55-064
33. Johnson PB, Christy RW. Optical constants of the noble metals. *Phys Rev B*. (1972) 6:4370–9. doi: 10.1103/PhysRevB.6.4370
34. Garcia MA, de Ia Venta J, Crespo P, LLopis J, Penades S, Fernandez A, et al. Surface plasmon resonance of capped au nanoparticles. *Phys Rev B*. (2005) 72:241403. doi: 10.1103/PhysRevB.72.241403
35. Michel JP, Lacaze E, Alba M, de Boissieu M, Gailhanou M, Goldmann M. Optical gratings formed in thin smectic films frustrated on a single crystalline substrate. *Phys Rev E*. (2004) **70**:011709. doi: 10.1103/PhysRevE.70.011709
36. Michel JP, Lacaze E, Goldmann M, Gailhanou M, de Boissieu M, Alba M. Structure of smectic defect cores: x-ray study of 8CB liquid crystal ultrathin films. *Phys Rev Lett*. (2006) **96**:027803. doi: 10.1103/PhysRevLett.96.027803
37. Zappone B, Lacaze E. Surface-frustrated periodic textures of smectic- a liquid crystals on crystalline surfaces. *Phys Rev E Stat Nonlin Soft Matt Phys*. (2008) **78**:061704. doi: 10.1103/PhysRevE.78.061704
38. Goubet N, Richardi J, Albouy PA, Pileni MP. Which forces control supracrystal nucleation in organic media? *Adv Funct Mater*. (2011) **21**:2693–704. doi: 10.1002/adfm.201100382
39. Gauvin M, Wan YF, Arfaoui I, Pileni MP. Mechanical properties of Au supracrystals tuned by flexible ligand interactions. *J Phys Chem C*. (2014) **118**:5005–12. doi: 10.1021/jp411896c
40. Wen T, Zhang D, Wen Q, Liao Y, Zhang C, Li J, et al. Enhanced optical modulation depth of terahertzWaves by self-assembled monolayer of plasmonic gold nanoparticles. *Adv Opt Mat*. (2016) **4**:1974–80. doi: 10.1002/adom.201600248
41. Lin S, Li M, Dujardin E, Girard C, Mann S. One-dimensional plasmon coupling by facile self-assembly of gold nanoparticles into branched chain networks. *Adv Mater*. (2005) **17**:2553–9. doi: 10.1002/adma.200500828
42. Bonell F, Sanchot A, Dujardin E, Péchou R, Girard C, Li M, et al. Processing and near-field optical properties of self-assembled plasmonic nanoparticle networks. *J Chem Phys*. (2009) **130**:034702. doi: 10.1063/1.3046291
43. Barrow SJ, Funston AM, Gómez DE, Davis TJ, Mulvaney P. Surface plasmon resonances in strongly coupled gold nanosphere chains from monomer to hexamer. *Nano Lett*. (2011) **11**:4180–7. doi: 10.1021/nl202080a
44. Mulvaney P. Surface plasmon spectroscopy of nanosized metal particles [Review]. *Langmuir*. (1996) **12**:788–800.
45. Voloschenko D, Pishnyak OP, Shiyanovskii SV, Lavrentovich OD. Effect of director distortions on morphologies of phase separation in liquid crystals. *Phys Rev E*. (2002) **65**:060701. doi: 10.1103/PhysRevE.65.060701
46. Schapotschnikow P, Pool R, Vlugt TJ. Molecular simulations of interacting nanocrystals. *Nano Lett*. (2008) **8**:2930–4. doi: 10.1021/nl8017862

47. Schapotschnikow P, Vlugt TJH. Understanding interactions between capped nanocrystals: Three-body and chain packing effects. *J Chem Phys*. (2009) **131**:124705. doi: 10.1063/1.3227043
48. Khan SJ, Pierce F, Sorensen CM, Chakrabarti A. Self-assembly of ligated gold nanoparticles: phenomenological modeling and computer simulations. *Langmuir*. (2009) **25**:13861–8. doi: 10.1021/la9008202
49. Pendery JS, Merchiers O, Coursault D, Grand J, Ayeb H, Greget R, et al. Gold nanoparticle self-assembly moderated by a cholesteric liquid crystal. *Soft Matt*. (2013) **9**:9366–75. doi: 10.1039/c3sm51736e
50. Qi H, Hegmann T. Multiple alignment modes for nematic liquid crystals doped with alkylthiol-capped gold nanoparticles. *ACS Appl Mater Interfaces*. (2009) **1**:1731–8. doi: 10.1021/am9002815
51. Khatua S, Manna P, Chang WS, Tcherniak A, Friedlander E, Zubarev ER, et al. Plasmonic nanoparticles liquid crystal composites. *J Phys Chem C*. (2010) **114**:7251–7. doi: 10.1021/jp907923v
52. Draper M, Saez I, Cowling S, Gai P, Heirich B, Donnio B, et al. Self-assembly and shape morphology of liquid-crystalline gold metamaterials. *Adv Funct Mat*. (2011) **21**:1260–78. doi: 10.1002/adfm.201001606
53. Kléman M. *Points, Lignes, Parois dans les Fluides Anisotropes et les Solides Cristallins. No. vol. 1 in Points, lignes, parois dans les fluides anisotropes et les solides cristallins*. Orsay: Éditions de physique (1977).
54. Holyst R, Oswald P. Dislocations in uniaxial lamellar phases of liquid crystals, polymers and amphiphilic systems. *Int JMod Phys*. (1995) **9**:1115–573.
55. Zhang C, Grubb AM, Seed AJ, Sampson P, Jákli A, Lavrentovich OD. Nanostructure of edge dislocations in a smectic-C* liquid crystal. *Phys Rev Lett*. (2015) **115**:087801. doi: 10.1103/PhysRevLett.115.087801
56. Repula A, Grelet E. Elementary edge and screw dislocations visualized at the lattice periodicity level in the smectic phase of colloidal rods. *Phys Rev Lett*. (2018) **121**:097801. doi: 10.1103/PhysRevLett.121.097801
57. Jain PK, Huang W, El-Sayed MA. On the universal scaling behavior of the distance decay of plasmon coupling in metal nanoparticle pairs: a plasmon ruler equation. *Nano Lett*. (2007) **7**:2080–8. doi: 10.1021/nl071008a
58. Thoen J, Marynissen H, Van Dael W. Temperature dependence of the enthalpy and the heat capacity of the liquid-crystal octylcyanobiphenyl (8CB). *Phys Rev A*. (1982) **26**:2886–905.
59. Géminard JC, Laroche C, Oswald P. Edge dislocation in a vertical smectic film: line tension versus film thickness and Burgers vector. *Phys Rev E*. (1998) **58**:5923–5.

Conflict of Interest: The authors declare that the research was conducted in the absence of any commercial or financial relationships that could be construed as a potential conflict of interest.